# Simultaneous Monitoring of Multiple People's Vital Sign Leveraging a Single Phased-MIMO Radar

Zhaoyi Xu<sup>®</sup>, Graduate Student Member, IEEE, Cong Shi<sup>®</sup>, Tianfang Zhang, Shuping Li, Graduate Student Member, IEEE, Yichao Yuan, Graduate Student Member, IEEE, Chung-Tse Michael Wu<sup>®</sup>, Senior Member, IEEE, Yingying Chen<sup>®</sup>, Fellow, IEEE, and Athina Petropulu<sup>®</sup>, Fellow, IEEE

Abstract—Vital sign monitoring plays a critical role in tracking the physiological state of people and enabling various healthrelated applications (e.g., recommending a change of lifestyle, examining the risk of diseases). Traditional approaches rely on hospitalization or body-attached instruments, which are costly and intrusive. However, in recent years there is an emergence of contactless vital sign monitoring techniques that rely on radio frequency signals. Early studies with continuous wave radars/WiFi devices have shown good success in detecting the vital signs of a single individual, while simultaneous monitoring of the vital signs of multiple, closely spaced subjects remains a challenge. In this paper, using an off-the-shelf Texas Instrument automotive FMCW radar, we design and implement a time-division multiplexing (TDM) phased-MIMO radar sensing system that allows high-precision vital sign monitoring of multiple subjects. The proposed sensing system can steer the beam towards the desired directions with a micro-second delay. The steerable beam enables capturing the vital signs of multiple individuals at the same radial distance to the radar. The proposed system enables the formation of a virtual array with aperture longer than that of the physical array. A Capon beamformer is used at the receiver side to combine the data collected from different transmit and receive antenna pairs corresponding to the virtual array. As all those pairs provide independent information about the targets, their combination significantly boosts the receiver signal-to-noise ratio. Based on the designed TDM phased-MIMO radar, we develop a system to automatically localize multiple human subjects and estimate their vital signs. Extensive evaluations show that under two-subject scenarios, our system can achieve more than 98.06% accuracy for breathing rate (BR) and more than 82.89% accuracy for heartbeat rate (HR) estimation, at a subject-to-radar distance of 1.6 m when the targets are facing the radar. The minimal subjectto-subject angle separation is 30° at a subject-to-radar distance of 1.6 m, corresponding to a close distance of 0.3 m between two subjects, which outperforms the state-of-the-art.

Manuscript received 30 September 2021; revised 13 December 2021 and 4 January 2022; accepted 8 January 2022. Date of publication 18 February 2022; date of current version 23 August 2022. This work was supported by NSF under Grants ECCS-2033433 and ECCS-1818478. (Corresponding author: Athina Petropulu.)

The authors are with the Department of Electrical and Computer Engineering, Rutgers The State University of New Jersey, New Brunswick, NJ USA (e-mail: zhaoyi.xu@rutgers.edu; cs1421@scarletmail.rutgers.edu; tz203@scarletmail.rutgers.edu; s11567@scarletmail.rutgers.edu; yy470@scarletmail.rutgers.edu; ctm.wu@rutgers.edu; yingche@scarletmail.rutgers.edu; athinap@soe.rutgers.edu).

This work involved human subjects or animals in its research. Approval of all ethical and experimental procedures and protocols was granted by Arts and Sciences IRB under Application No.: Pro2021002083, and performed in line with the Multi-target Physiological Detection using AWR2243.

Digital Object Identifier 10.1109/JERM.2022.3143431

Index Terms—Contact-less vital sign monitoring, millimeter wave, phased multiple-input multiple-output radar.

#### I. Introduction

RACKING of the physiological states of people can enable change of lifestyle recommendations and examine the risk of diseases. Vital signs, including breathing rate (BR) and heartbeat rate (HR), provide crucial insights into the physiological state of the individual. Traditional ways to monitor vital signs usually require hospitalization and involve body-attached instruments (e.g., PPG and ECG sensors), which are intrusive, costly, and require the cooperation of the person being monitored. To overcome these problems, research studies have been exploring contact-less vital sign monitoring via radio frequency (RF) signals [1]–[5]. Early studies used continuous-wave radar, or WiFi devices transmitting RF signals. The signal echoes are modulated by the small chest movements caused by those vital signs, thus can be used for vital sign estimation [6], [7], [27]. However, the methods of [6], [7] rely on RF signals that operate at fixed frequencies, and thus have limited ability to disentangle echo signals from targets at different ranges. Such limitation precludes their use in health monitoring of multiple individuals, for example, they could not be used for tracking the vital signs of people in the over-crowded, resource limited clinics that we experienced during the COVID-19 crisis. In [27], sophisticated signal processing techniques were used along with a commercial 60 GHz WiFi device transmitting OFDM signals. OFDM signals provide the ability to resolve targets from different range bins.

Powered by recent advances in mmWave sensing, research studies have been exploring mmWave signals for vital sign monitoring [8]–[16]. Compared to low-frequency RF signals[17], mmWave signals have much shorter wavelength, and thus can better respond to small chest movements, enabling more fine-grained vital sign monitoring. By utilizing frequency-modulated continuous-waveform (FMCW) techniques, a mmWave radar can detect multiple people at different radial distances to the radar device, and further derive vital signs information of each individual.

MmWave FMCW radar for vital sign monitoring has been explored via phased arrays, performing analog beamforming, or multiple-input and multiple-output (MIMO) radar. The phased

array approach of [8], [11] uses analog beamforming to successively steer the mmWave beam towards different directions. This is achieved by varying the antenna weights so that the transmitted energy is focused in the desired direction. Those works enable the detection of people separated in the angle domain, while the allowable minimum angle separation (resolution) is limited by the receive array's aperture. By processing the echoed signals of each beam separately, the vital signs of the person in each direction can be estimated. Specifically, [11] deploys analog beamforming on a single-channel FMCW radar to measure the vital signals of two subjects at different ranges with minimum angle separation of 40 degrees. However, [11] reported preliminary BR and HR estimation performance of a single subject only (i.e., around 93% HR estimation and 96% BR estimation accuracy). Using a MIMO radar approach, [12] transmits mmWave signals via multiple transmitting antennas (TX) in a time-division-multiplexing (TDM) fashion, and use multiple receiving antennas (RX). By leveraging the TDMinduced orthogonality of the transmitted signals, each receive antenna can extract the contribution of each transmit antenna. The contributions of different TX-RX pairs offer independent views of the targets, which can be exploited to improve target estimation. For example, [12] uses a MIMO radar with 12 TXs and 16 RXs, where in each time slot, only one of the available TXs transmits. The measurements collected over 12 slots correspond to 192 TX-RX antenna pairs, and can be used for high-precision vital sign monitoring with low estimation error. Similarly, [16] presented results using an FMCW-based MIMO radar with 8 TXs and 16 RXs. All the aforementioned methods consider either analog beamforming, or MIMO techniques, but not both, thus missing the opportunity to fully explore the potential of radar-based mmWave sensing.

In this paper, we propose a novel approach for high-precision vital sign monitoring of multiple people that uses techniques that have not been explored before for vital sign monitoring. In particular, we propose a TDM phased-MIMO radar sensing scheme that performs transmit and receive beamforming. We also propose an implementation of the proposed scheme using as basic tool a single-chip automotive mmWave FMCW antenna array and present results for monitoring of the vital signs of two subjects. The unique features of the proposed radar are the following:

- i) In each time slot the proposed system transmits a waveform through a phased array structure. The antenna weights in each slot are chosen so that a beam, focusing the transmitted power to the desired direction, is formed. This assumes that the targets have been first detected and their angles are known.
- ii) The TDM-MIMO operation of the proposed system enables the formation of a virtual receiving array with aperture longer than that of the physical receiving array. As all transmit-receive pairs corresponding to the virtual array provide independent information about the targets, their combination significantly boosts the receiver signal-to-noise ratio allowing high precision target estimation.
- iii) A Capon beamformer (CB) [18] is implemented at the receiver, so that the receiving array focuses on echoes

coming from the desired directions, while the power from all other directions is minimized. The large aperture of the virtual receive array enables the receiver to separate closely spaced targets.

On establishing the relation of the proposed work to the above cited literature, we should note that [11] did not have features (ii) and (iii), while [12], [16] did not have features (i) and (iii).

Based on the proposed radar, we develop a system to automatically localize multiple human subjects and estimate their vital signs. Initially, our proposed system transmits as a TDM MIMO radar, and then uses Capon's beamformer on the virtual receiving array to obtain the angles of the targets with respect to the radar. Subsequently, it works as a TDM phased-MIMO radar, iteratively steering the beam towards each individual subject, one subject per slot. The received echoes corresponding to the same subject are processed through a receive Capon beamformer, which focuses on the echoes coming from the desired direction, while minimizing the power from other directions. The narrow beam from the large virtual array aperture enables the separation of the targets, so that each beam contains the vital signs of one subject only.

For each subject, our system computes the phase of range Discrete Fourier Transform (DFT) peaks corresponding to human subjects, which encodes both the breathing and heartbeats of the subject. Two band-pass filters, which use normal human breathing and heartbeat frequency ranges as cut-off frequencies, are employed to separate the two types of vital signs. Our system then detects the BR and HR in the frequency domain by locating the frequency peaks.

We implement the designed TDM phased-MIMO radar on an off-the-shelf Texas Instrument (TI) AWR2243 mmWave radar with 3 TXs and 4 RXs. Our phased-MIMO radar can steer the mmWave beam towards different directions with a micro-second delay, which enables simultaneously monitoring of the vital signs of multiple individuals. By combining high angle resolution and high precision target estimation, the proposed system enables the precise estimation of the BR and HR of multiple people located close to each other, even when they are at the same radial distance to the radar. We conduct extensive experiments involving two subjects, under various settings (e.g., different distances and angles between the radar and subjects). The results show that our system can provide high accuracy BR and HR estimation under various experimental settings. Our approach thus provides a promising solution to track the health status of multiple people in many indoor venues (e.g., classrooms, offices, and crowded hospital rooms).

#### II. THE PROPOSED TDM PHASED-MIMO RADAR

#### A. Analog Transmit Beamforming

A phased-MIMO radar combines MIMO radar and phased array features, in the sense that the radar transmits orthogonal FMCW signals (see Section II.C), each feeding a phase array structure. Here, orthogonality is achieved by TDM transmission of the same waveform, weighted by different weights in each slot. Orthogonality allows the transmitted signals to be separated at the receiver. The contributions of the multiple orthogonal

signals offer independent views of the targets, which can be exploited to improve target estimation.

Let us consider a transmitter that has a uniform linear array (ULA) with N TXs spaced by  $d_t$ , and a receiver that has a ULA with M RXs spaced by  $d_r$ . The transmit array transmits in a time-slotted fashion. In each slot, each TX transmits a weighted version of waveform x(t), using different weights between slots. The weights are chosen so that the transmissions of all antennas add up coherently in a specific direction. By using different weights in each slot we effectively create different channels that provide diversity and thus can lead to improved target estimation.

Let the weights for the p-th slot be

$$\mathbf{w}_{p}(\theta) = e^{j2\pi p\alpha(\theta)} [1, e^{-j2\pi\alpha(\theta)}, \dots, e^{-j2\pi(N-1)\alpha(\theta)}]^{T}$$
$$= e^{j2\pi p\alpha(\theta)} \mathbf{a}_{t}(\theta)$$
(1)

where  $\alpha(\theta)=d_t\frac{\sin(\theta)}{\lambda}$ ,  $\lambda$  is the wavelength of signal and  $\mathbf{a}_t(\theta)$  is the transmit steering vector. If  $\theta_0$  is the direction of the beam, the signal transmitted in the p-th slot towards direction  $\theta$  can be written as

$$z_p(t,\theta) = \mathbf{a}_t^H(\theta) \mathbf{w}_p(\theta_0) x(t)$$
  
=  $e^{j2\pi p\alpha(\theta)} \mathbf{a}_t^H(\theta) \mathbf{a}_t(\theta_0) x(t)$ , (2)

where  $\{\cdot\}^H$  denotes the conjugate transpose operation. The transmitted power towards direction  $\theta$  during the p-th slot equals

$$Q(\theta) = E\{z_p(t, \theta)z_p^H(t, \theta)\}$$
$$= |b(\theta)|^2 Q_x \tag{3}$$

where  $b(\theta) = \sum_{n=0}^{N-1} e^{j2\pi n[\alpha(\theta)-\alpha(\theta_0)]}$ , and  $Q_x$  is the basedband signal power. One can see that  $b(\theta_0) = N$ , and the transmitted power is maximized along direction  $\theta_0$ . Also, the signal transmitted in each slot is the same as that of a TDM-MIMO radar using the same array, except that it is amplified by the number of antennas.

We should note that analog beamforming (see Eq. (1)) is not optimal, in the sense that although it makes the signals add up in phase in the preferred direction, it does not control the power along other directions. Optimal transmit beamforming would modulates the power of each TX as well as the phase, and thus could control the sidelobe level. However, optimal transmit beamforming is hard to implement on a phased array.

#### B. Virtual Array and Receive Beamforming

Let us assume that the target is at direction  $\theta_0$ . After mixing the received signal with the conjugate of the transmitted signal, the beat signal [28] in the p-th slot is

$$\mathbf{y}_p(t) = \mathbf{a}_r(\theta_0) z_p(t - \tau, \theta_0) x^H(t)$$
(4)

where  $\mathbf{a}_r(\theta) = [1, e^{-j2\pi d_r \frac{\sin \theta}{\lambda}}, \dots, e^{-j2\pi (M-1)d_r \frac{\sin \theta}{\lambda}}]$  is the receive steering vector and  $\tau$  is the round-trip delay. By stacking the received signal from P slots, one can formulate a virtual array of  $P \cdot M$  elements with steering vector

$$\mathbf{a}_v(\theta) = \mathbf{a}_r(\theta_0) \otimes [1, \dots, e^{j2\pi(P-1)\alpha(\theta_0)}]^T$$
 (5)

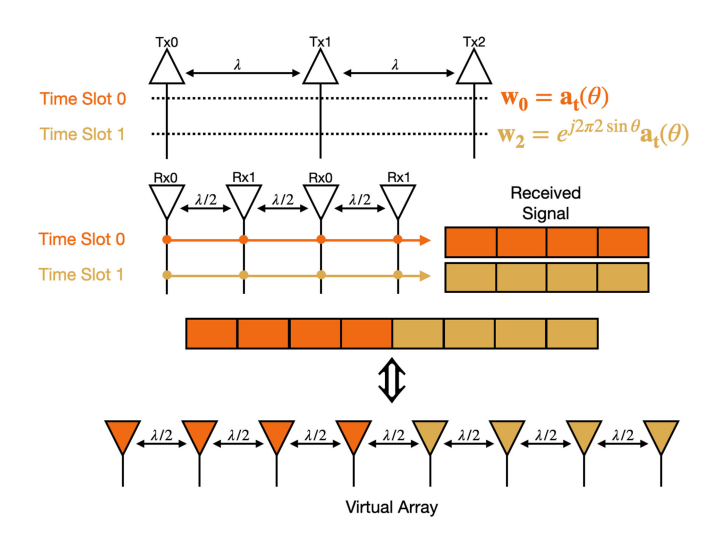


Fig. 1. A TDM phased-MIMO with 3 TX and 4 RX gives rise to a receiving virtual uniform linear array with 8 RX antennas. This provides 8 TX-RX pairs for target estimation.

where  $\otimes$  denotes the Kronecker product. Thus the virtual array provides a larger aperture than that of the physical receive array. The output of the virtual array is

$$\mathbf{y}_{v}(t) = N\mathbf{a}_{v}(\theta)x(t-\tau)x^{H}(t) \tag{6}$$

Let us apply CB on the virtual array output. This will allow us to focus on signals coming form the desired direction,

$$z(t) = \mathbf{w}_v^H \mathbf{y}_v(t) \tag{7}$$

where

$$\mathbf{w}_{v} = \frac{\mathbf{R}_{y}^{-1} \mathbf{a}_{v}(\theta)}{\mathbf{a}_{v}^{H}(\theta) \mathbf{R}_{y}^{-1} \mathbf{a}_{v}(\theta)}$$
(8)

with  $\mathbf{R}_y$  being the received signal covariance matrix (please refer to Section II-C for estimation details).

An example of TDM phased-MIMO is shown in Fig. 1 where the system has 3 TXs spaced apart by a wavelength, and 4 RXs spaced apart by half of wavelength. Two time slots are used to formulate a TDM phased-MIMO with 8 virtual elements. The corresponding 3-dB beam width for such configuration is 18° which supports at maximum 11 non-overlapped beams with distinct directions in a field of view of 180° to monitor vital signals.

By exploiting the multiple channels, corresponding to the multiple TX-RX antenna pairs of the virtual array, phased-MIMO can achieve higher target resolution and higher SNR than a phased array. Also, by implementing transmit beamforming, phased-MIMO can avoid clutter. In vital sign monitoring applications, especially in the multi-target scenario, phased-MIMO can steer the beam towards each of the target and individually monitor their vital signals even when the targets are closely spaced. As shown in Section IV-D, phased-MIMO can achieve good performance when the targets are closely placed and with different orientations.

### C. FMCW Waveforms and Target Parameter Estimation

The proposed radar uses FMCW waveforms, i.e., the transmitted signal is given by (2), where

$$x(t) = A_t e^{j2\pi [f_c t + \frac{B}{2T_c} t^2 + \Phi(t)]}.$$
 (9)

In the above,  $A_t$  is the amplitude,  $f_c$  is the chirp starting frequency, B is the chirp bandwidth,  $T_c$  is the chirp duration, and  $\Phi(t)$  is the phase noise from the transmitter. Note that the phase noise will be neglected in the following equations since it is slow varying and the propagation delay of mmWave is small.

The transmitted signals in all time slots will be referred to as a frame. Multiple frames are transmitted in sequence to monitor the vital signals of subjects. At the radar receiver, based on (6), the signal received by the m-th RX, due to the transmission of the n-th antenna, i.e., the (nN+m)th element of  $\mathbf{y}_v(t)$ , can be written as

$$y(n, m, t) = A_{nm} e^{-j2\pi [f_b t + \Phi_b(t, n, m)]},$$
(10)

where  $A_{nm}$  is the complex amplitude of the signal transmitted by the n-th transmit antenna and received by the m-th receive antenna after beamforming, and also contains the effect of the path between the two antennas,  $f_b = \frac{2BR(t)}{cT_c}$  is the beat frequency,

$$\Phi_b(t,n,m) = \frac{2f_c R(t)}{c} - \frac{2BR^2(t)}{c^2 T_c} - (d_m - d_n) \frac{\sin(\theta)}{\lambda},$$

R(t) is the radial range of the subject, which is associated and changed with the chest displacements of the target,  $d_n=(n-1)d_t$  and  $d_m=(m-1)d_r$ , respectively. Since the propagation delay is very small, the phase term can be approximated as  $\Phi_b(t,n,m)=\frac{2f_cR(t)}{c}-(d_m-d_n)\frac{\sin(\theta)}{\lambda}$ . Using discrete-time samples, based on ADC sample interval

Using discrete-time samples, based on ADC sample interval  $T_s$  and frame interval  $T_f$ , the signal of (10) corresponding to the k-th ADC sample of the l-th frame can be written as

$$y[n, m, k, l] = A_{nm} e^{j2\pi [f_b k T_s + \frac{2f_c}{c} R(k T_s + l T_f) - (d_m - d_n) \frac{\sin(\theta)}{\lambda}]}.$$
(11)

Provided that the range change due to vital sign is slow (< 2Hz) and the sampling interval is very short, if the target stays at a nominal range  $R_0$ , then the phase term of (11) will be

$$\Phi_b(l, n, m) = \frac{2}{\lambda} [R_0 + R_1(lT_f)] - (d_m - d_n) \frac{\sin(\theta)}{\lambda}$$

$$= \Phi_0(n, m) + \frac{2R_1(lT_f)}{\lambda}.$$
(12)

where  $R_1(l)$  denotes the chest displacement due to vital activities and (11) can be expressed as

$$y[n, m, k, l] = A_{nm} e^{j2\pi\Phi_0(n,m)} e^{j2\pi f_b k T_s} e^{j2\pi \frac{2R_1(lT_f)}{\lambda}}.$$
 (13)

The virtual array is formulated as follows

$$\mathbf{y}_{v}(k,l) = [y[0,0,k,l], y[0,1,k,l],$$

$$\dots, y(N-1,M-1,k,l)]^{T}.$$
(14)

To compute the optimal CB weights (see (8)), we need to obtain an estimate of the covariance matrix based on the

available data, i.e.,

$$\hat{\mathbf{R}}_{y}(l) = \frac{1}{K} \sum_{k=0}^{K-1} \mathbf{y}_{v}(k, l) \mathbf{y}_{v}^{H}(k, l)$$
 (15)

and then use that as the true covariance in (8). Then the CB output equals

$$z[k,l] = \mathbf{w}_v^H(l)\mathbf{y}_v(k,l)$$
$$= \tilde{A}e^{j2\pi\frac{2R_1(lT_f)}{\lambda}}e^{j2\pi f_b kT_s}.$$
(16)

where  $\tilde{A} = \sum_{n=0}^{N-1} \sum_{m=0}^{M-1} A_{nm}$ . One can clearly see that even if some  $A_{nm}$  are close to zero due to bad channels,  $\tilde{A}$  will be non-zero and as a result, the CB output will be non-zero. This is the advantage of using the multiple TX-RX pairs provided by the virtual array. Thus, the subsequent estimation of vital sign signals enjoys high SNR. Our system then leverages the combined signal z[k,l] for BR and HR estimation.

The signal consisting of K samples of z[k,l] during the l-th frame, i.e.,  $z[k,l], k=0,\ldots,K-1$  can be viewed as a complex sinusoid with frequency  $f_bT_s$  and complex amplitude  $\tilde{A}e^{j2\pi\frac{2R_1(lT_f)}{\lambda}}$ . Therefore, on applying a K-point DFT on z[k,l] along k we see a peak at DFT sample  $h=\lfloor Kf_bT_s\rfloor$  where  $\lfloor \cdot \rfloor$  refers to the floor function, indicating the radial range of the target [19]. The phase of  $\tilde{A}$  is constant and can be estimated (see Section III-B) by observing the phases of the peak value in all frames. Thus, based on the phases of the DFT sample  $h=\lfloor Kf_bT_s\rfloor$ , i.e.,  $arg\{\tilde{A}\}+2\pi\frac{2R_1(lT_f)}{\lambda}$  for  $l=0,\ldots,L$ , one can measure the frequency of chest displacement caused by human chest displacements. In this paper, we use the real and imaginary parts of the peak corresponding to the target in the l-th frame, denoted as  $Y_R[l]$  and  $Y_I[l]$ .

# III. IMPLEMENTATION ISSUES OF VITAL SIGN MONITORING SYSTEM

#### A. Target Detection

Prior to applying the TDM phased-MIMO technique for multi-people vital sign monitoring, we need to detect the human subjects and determine their angles with respect to the radar. For this purpose the radar first works as a TDM MIMO radar where only one antenna is active in each slot. Then on the received echos we use CB, a widely used angle estimation method, which provides better resolution as compared to conventional methods [8].

Upon detecting one or more target subjects, our system steers the mmWave beam towards the directions of the detected targets by applying analog beamforming at the TX side. Our system then utilizes CB, phased calibration, and frequency analysis techniques as described below to estimate the vital signs of the target subjects.

# B. Constellation Correction With Least-Square

Due to the strong coupling effects and interference in the measurement environment, the range DFT outputs usually contain DC offsets, which distort the phase information at the target's range bin. It is thus necessary to remove the DC offsets before

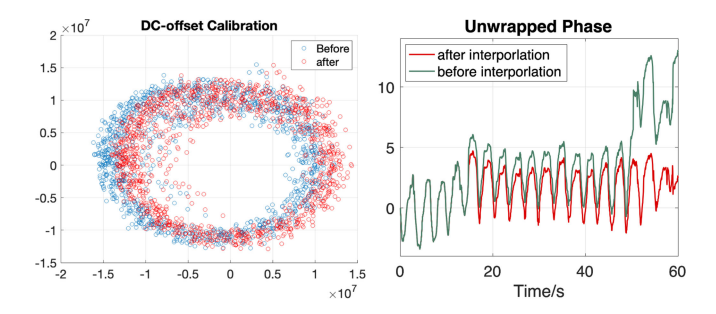


Fig. 2. (a) DC-offset correction using least square method; (b) Phase drift calibration through interpolation.

we deriving reliable vital sign information. Given a TX-RX pair, i, the phase at a selected range bin h can be formulated as

$$\phi(l) = \arctan\left[\frac{Im(r_{i,h}(l) + DC_{im})}{Re(r_{i,h}(l) + DC_{re})}\right],\tag{17}$$

where  $DC_{im}$  and  $DC_{re}$  denote the imaginary and real parts of the complex DC offset, respectively.  $r_{i,h}(l)$  shows the range DFT output of the combined signal z[k,l] at range bin h in the l-th frame. The formulation indicates that the DC offset will shift the origin to  $(DC_{re}, DC_{im})$ . To compensate such a shift, we use the least-squares method to estimate and cancel  $(DC_{re}, DC_{im})$  [9]. An example is shown in Fig. 2(a) where the shifted phases (red dots) are moved so that the center is at the origin (blue dots).

#### C. Phase Calculation With DACM

Existing work [20] found that the human chest displacement can exceed the wavelength of mmWave signals (i.e., <4 mm for 77 GHz). Therefore, the phase of the range DFT can be outside the range  $[-\pi,\pi]$ , which can lead to false detection of vital signs. To tackle this issue, we use the differential and cross-multiply algorithm (DACM) [29] to calculate phase.

Instead of directly applying arctangent demodulation, DACM converts complex range DFT outputs of l-th frame into phases leveraging the derivative of arctangent function

$$\phi(l) = \phi(l-1) + \Delta\phi(l), \quad l = 2, 3, \dots, L,$$
 (18)

where L is the number of frames and

$$\Delta\phi(l) = \frac{Y_R[l]\{Y_I[l] - Y_I[l-1]\} - \{Y_R[l] - Y_R[l-1]\}Y_I[l]}{Y_R[l]^2 + Y_I[l]^2}.$$

The DACM algorithm mainly corrects the phase distortions caused by breathing. In contrast, small-scale heartbeat motions are less likely to exceed the range of phase.

# D. Phase Drift Calibration Based on Phase Difference

Signal phase drifts in transmission, mainly caused by the impacts of temperature and humidity variations on the hardware, make the range of phase fluctuations exceed the normal ranges of human breathing and heartbeat. The phase drifts cannot be removed leveraging DACM, since these drifts can be close to but not exceeding the unwrapping threshold of  $\pm\pi$ . Furthermore, the harmonics of breathing [21] (i.e., multiple of breathing frequency, e.g., 0.2-0.33Hz) can also distort the phase patterns at the heartbeat frequency range (e.g., 0.8-2.0Hz).

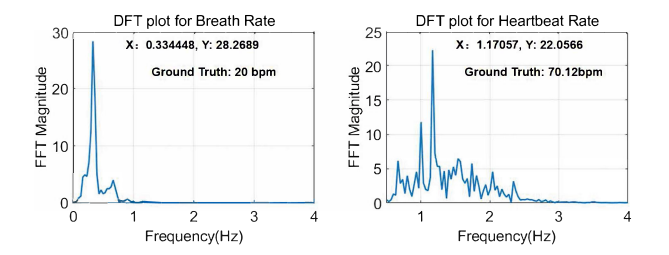


Fig. 3. BR and HR estimation by applying frequency analysis on the phase of mmWave signals.

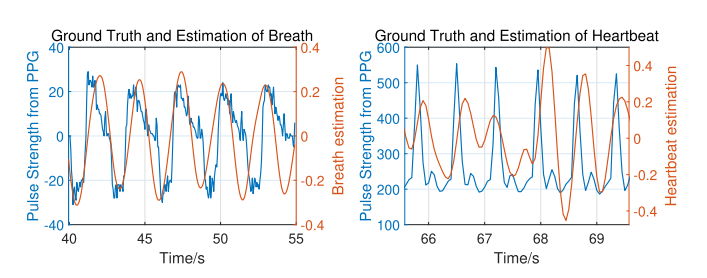


Fig. 4. Comparison between ground truth and our estimation on breath and heartbeat.

It is thus necessary to remove the impacts of such harmonics for reliable HR estimation. For that purpose, we realize phase drift calibration [8] by computing the phase difference  $\Delta\phi(l)=\phi(l)-\phi(l-1)$  for each  $\phi(l).$  If the absolute value of the phase difference exceeds a certain threshold,  $\phi(l)$  will be replaced by a new value computed by the Lagrange interpolation of the previous three phases  $\phi(l-3),\phi(l-2),\phi(l-1).$  An example is shown in Fig. 2(b).

# E. BR and HR Estimation

We apply frequency analysis upon the calibrated phase within a sliding window to estimate BR and HR. Since the periods of human breathing and heartbeat are close to each other, we need to separate the BR and HR for reliable estimations. Particularly, we apply a 3-th order Butterworth bandpass filter with a cut-off frequency range of 0.8 - 2.0Hz to extract heartbeats, which removes the impacts of human breathing and its harmonics. Similarly, we use another bandpass filter of 0.1 - 0.5Hz to extract human breaths. Then, our system applies a DFT on the extracted breathing signals, and takes the highest peak of the DFT magnitude as the detected BR. To extract heartbeat, which involves subtler displacement, we first calculate phase difference:  $\Delta \phi(l) = \phi(l) - \phi(l-1)$ , which reveals minor phase changes [22]. Our system then applies a DFT on the phase differences to calculate the HR. Examples of BR and HR estimation results are shown in Fig. 3. Comparisons between ground truth and our estimation of breath and heartbeat are shown in Fig. 4.

#### IV. PERFORMANCE EVALUATION

#### A. TDM-Phased-MIMO Implementation

As a proof of concept, we implement the proposed TDM phased-MIMO radar on an off-the-shelf TI AWR2243 mmWave device [23], [24], which transmits and receives FMCW waveforms within  $76GHz \sim 81~GHz$  frequency range. As shown

TABLE I
CHIRP PARAMETERS USED IN THIS WORK

Start Frequency, $f_c(GHz)$	77
Frequency Slope, S (MHz/µs)	29.982
Idle Time (μs)	100
TX Start Time (μs)	0
ADC Start Time(μs)	6
ADC Samples	256
ADC Sample Rate (MHz)	10
Ramp End Time (µs)	60
Number of Subframe Per Frame	2/4
Number of chirp Per Subframe	1
Slow-time Sampling Frequency, $f_s=1/T_s$ (Hz)	20
Subframe Periodicity (ms)	12.5
Frame Periodicity (ms)	50

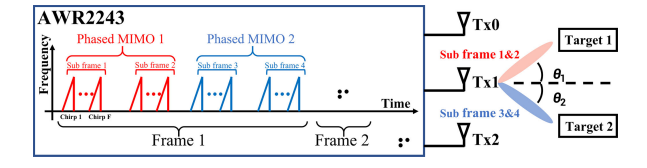


Fig. 5. Subframe implementation on AWR2243 (F=1).

in Fig. 1, the mmWave device consists of three TXs with the spacing of  $\lambda$  and four RXs with the spacing of  $\lambda/2$ , respectively. It is noted that while the middle TX antenna element is offset from the other two in the elevation direction [23], the antenna array can still be assumed as a linear antenna array in the horizontal direction given the broadside radiation of the patch antennas and wavefront direction. In the measurement setup, each TX chain includes a programmable phased shifter, with which the analog scanning angle can be achieved by providing different phase information feeding to each TX, separately. The FMCW setting based on AWR2243 was shown in Table I. In this configuration,the resolution of range bin measurement is 19.5 cm. An evaluation board TI DCA1000 [25] is adopted in the streaming mode to acquire raw baseband I/Q signals down-converted from received signals.

It is worth mentioning that when leveraging TXs to realize the analog beamforming, there will be grating lobes pointing to other directions because of the large spacing between TXs,  $\lambda > \lambda/2$ , which may introduce interference in the multi-target scenario. Nevertheless, RXs are spaced by  $\lambda/2$  which means there is no grating lobe at the receiver side. By leveraging the CB at the receiver side, we can alleviate the grating lobe problem since the energy is focused to a certain direction. In multiplesubject scenarios, our TDM phased-MIMO radar can change the beam direction towards two different subjects within one frame periodicity of 50 ms. Each frame is equally divided into four subframes [26] for multi-target detection, whose block diagram is shown in Fig. 5. Particularly, the direction 1 can be illuminated using subframe 1 with TX0 as the reference, and subframe 2 with TX2 as the reference, while the direction 2 can be illuminated using subframe 3 with TX0 as the reference and subframe 4 with TX2 as the reference.

## B. Experimental Validation and Error Analysis

We evaluate the performance of our vital sign monitoring system under single-subject and two-subject scenarios. For both

TABLE II
REPRESENTATIVE RESULTS OF BREATH RATE ESTIMATION (SINGLE TARGET SCENARIO AND MULTI-TARGET SCENARIO)

Users	Users Distance and Angle	Breath Rate Estimation Results (BPM)		
Osers Distance and Ar	Distance and Angle	Phased-Array	Phased-MIMO	PPG (Ground Truth)
User 1	1.5m, 30°	19.03	20.03	20.01
User 2	3.0m, -10°	18.03	16.03	16.34
User 1(User 3)	1.5m(3.0m), 30°(-10°)	18.05 (19.03)	16.96 (20.00)	17.37 (20.05)
User 3(User 4)	2.0m(2.0m), 10°(-30°)	18.67 (17.02)	16.56 (18.03)	16.12 (18.14)

TABLE III
REPRESENTATIVE RESULTS OF HEARTBEAT RATE ESTIMATION (SINGLE TARGET SCENARIO AND MULTI-TARGET SCENARIO)

	Users	Distance and Angle	Heartbeat Rate Estimation Results (BPM)		
	Distance and Angle	Phased-Array	Phased-MIMO	PPG (Ground Truth)	
Ì	User 1	1.5m, 30°	62.89	84.46	84.07
1	User 2	3.0m, -10°	61.11	61.33	61.14
Ì	User 1(User 3)	1.5m(3.0m), 30°(-10°)	78.22 (72.10)	77.62 (70.81)	78.06 (70.83)
	User 3(User 4)	2.0m(2.0m), 10°(-30°)	65.82 (65.04)	66.02 (71.37)	67.05 (72.06)

scenarios, we conduct experiments to study the impacts of various factors, including the distance between the radar and the subject and the separation angle between two subjects and the orientations of subjects. A total of 40 experiments was conducted, each of 2 min time duration. A total of 6 volunteers participated in the experiments. As ground truth we use breathing and heartbeat signals collected with a Neulog NUL236 respiration belt and a Neulog NUL208 Heart Rate sensor. A 60-second sliding window, with a step size of 1 s, is applied upon the breathing and heartbeat signals to obtain the ground-truth BR and HR. We compare the HR and BR estimates obtained with our proposed system to the ground truth. To quantify the vital sign estimation performance, we use statistical metrics including standard derivation (STD), root-mean-square error (RMSE), and estimation accuracy, which are also used in prior work [9]. Specifically, STD indicates the consistency of the estimations, and a lower STD means higher consistency and better performance. RMSE measures the average errors between the estimations of our system and the ground truth. Besides these two statistical metrics, we use estimation accuracy for evaluation, which is defined as the percentage of the estimation with < 3 bpm errors.

# C. Single-Target Vital Sign Estimation

In the scenario of single-target vital sign monitoring, the subject is requested to sit in front of the radar, which is placed 1 m, 2 m and 4 m away from the subject with a direction of  $20.1^{\circ}$ . The estimation accuracy and statistic results of single-target BR are shown in Fig. 7. Results of single-target breath and heartbeat estimation are shown in Table II and Table III. For the single-target BR estimation on 1 m and 2 m, the estimation accuracy for phased-array can reach 97%. However, under a far radar-to-subject distance of 4 m, the accuracy drops to 80% for predictions of  $< 3 \ bpm$  errors. In contrast, the phased-MIMO not only maintains high accuracy on BR estimation on 1 m (99%) and 2 m (100%), but achieves much higher accuracy at 4 m, with 100% for predictions of  $< 3 \ bpm$  errors as well. For the statistic results, the STD and RMSE of both phased-array and phased-MIMO experience a severe increasing when the distance between subjects and radar increases to 4 m, which can attribute to the instability of long distance data collection from radar.



Fig. 6. Setup for multi-target vital sign monitoring.

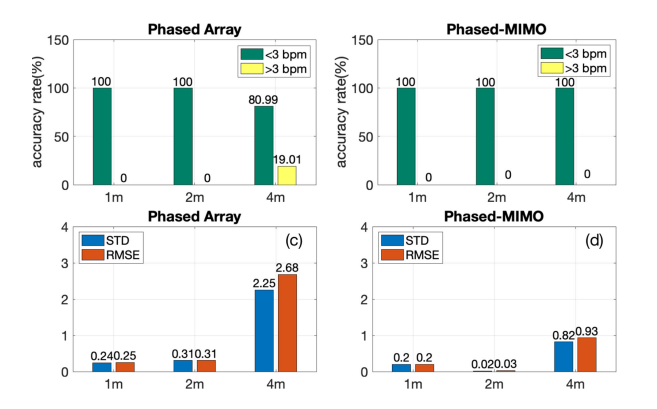


Fig. 7. (a), (b) Accuracy on single-target BR estimation; (c), (d) corresponding errors. X-axis: subject-to-radar distance.

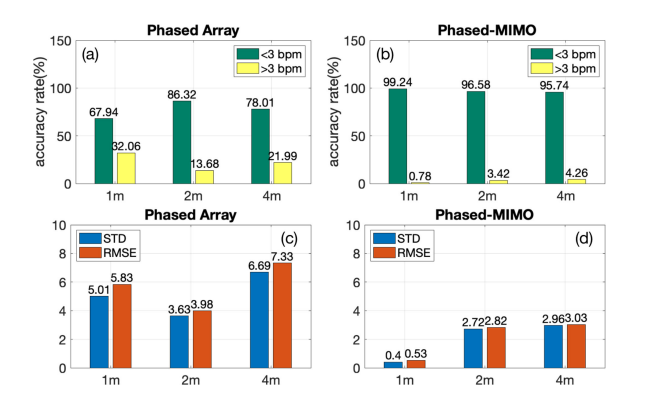


Fig. 8. (a), (b) Accuracy on single-target HR estimation; (c), (d) corresponding errors. X-axis: subject-to-radar distance.

Compared to phased-array, phased-MIMO has much lower STD and RMSE on all three different distances, demonstrating the superior performance on BR estimation.

In Fig. 8, we compare the performance of phased array and proposed phased-MIMO on HR estimation. For phased-array, the accuracies are only 67.9%, 86.3%, and 78.0%, at 1 m, 2 m, and 4 m, respectively. In contrast, the proposed phased-MIMO has much better HR estimation performance, with over 95% accuracy at three different distances. We note that phased array has the best performance on the setup of 2 m, with STD of 3.63 and RMSE of 3.98. In order to illustrate this observation, we draw a schematic in Fig. 9, where the human body is approximated as a circle with 0.44 m of diameter. As shown in Fig. 9, due to the width of human, when the targets are at 1 m, the beam formulated by the phased array does not cover the whole chest thus leading to a low accuracy. At 2 m, the beam covers the whole chest, and thus a higher accuracy is achieved. At 4 m, due to attenuation of mmWave signal, the accuracy is lower than in the 2 m case. With the combination of 8 channels,

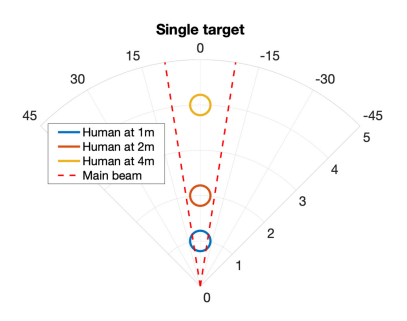


Fig. 9. Beam formulated by phased array with 3 TX can not cover the whole body when target is 1 m far from radar.

even at longer distance the proposed phased-MIMO has lower STD and RMSE, which proves the stability and robustness using phase-MIMO to make single-target heartbeat estimation.

### D. Multi-Target Vital Sign Estimation

Multi-target vital signs detection is more challenging, especially when the targets are in the same range bin, since the FMCW signal only provides range information [9]. For that case, we propose to use analog beamforming and CB to separate different targets in the angle domain. By transmitting beams towards each of the target, we can isolate the targets at the same distance; by CB on the virtual array, we can further focus the energy of received signal towards the desired target and thus reduce the interference from other targets. In the first multi-target detection experiment, two targets are sitting along the direction of  $-30^{\circ}$  and  $30^{\circ}$  with the same distance of 1 m or 1.6 m away from the radar sensor. In this case, due to the large spacing between TXs, the grating lobe issue appears along the direction of  $-30^{\circ}$  with the maximum gain of main beam along the direction of 30° and vice versa. Fortunately, we can use CB on the virtual array to address this problem.

Example results of multi-target breath and heartbeat estimation are shown in Table II and Table III. The statistic result comparison between phased array and phased-MIMO are shown in Fig. 10, when two targets are located at different distances with the angle separation of 60°. In Figs. 10(a) and (b), for BR estimation, both the accuracy rates for the phased-MIMO and the phased array are 100%. At a distance of 1 m, the STD and RMSE of the phased array are 0.14 and 0.2, respectively, while the STD and RMSE for the proposed phased-MIMO are 0.06 and 0.15, respectively. At a distance of 1.6 m, the STD and RMSE for the phased array are 0.6 and 0.71, respectively, while the STD and RMSE for the phased-MIMO are 0.55 and 0.66, respectively. For HR estimation in Figs. 10(c) and (d), the accuracy rates between phased array and phased-MIMO are 40.68% and 87.29%, At a distance of 1 m, the STD and RMSE for phased array are 4.2 and 5.83, respectively, while the STD and RMSE of the phased-MIMO are 1.48 and 2.99, respectively. At a distance of 1.6 m, the STD and RMSE for the phased array are 9.88 and 14.17, respectively, while the STD and RMSE for the phased-MIMO are 1.31 and 1.53, respectively.

When two targets located at the distance of 1.6 m with different angle separations of  $40^{\circ}$ ,  $45^{\circ}$  and  $60^{\circ}$ , the performance of the phased array and the phased-MIMO are summarized in Fig. 11 and the experiment setup for  $45^{\circ}$  is shown in Fig. 6. In Figs. 11(a) and (b), for BR estimation, the accuracy rate of the

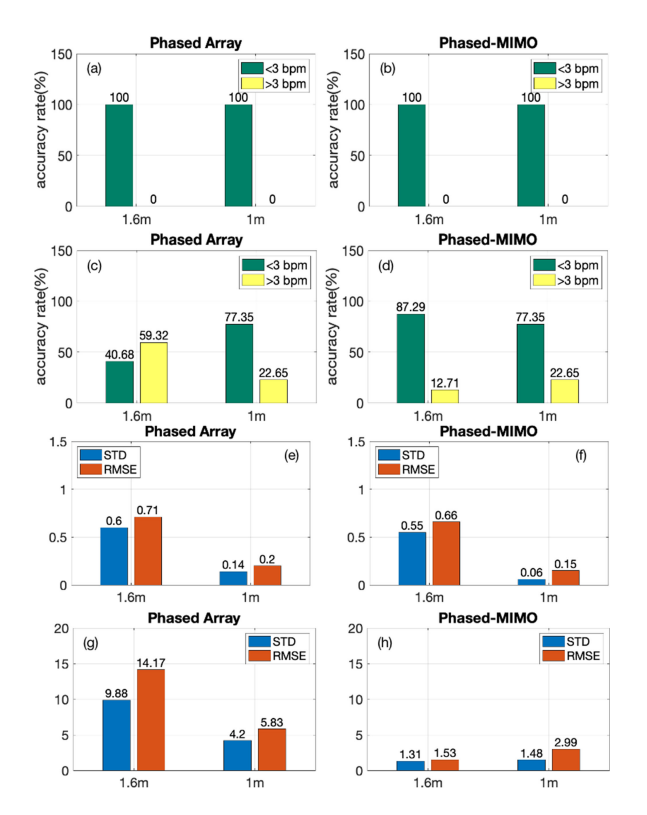


Fig. 10. (a), (b) Accuracy on multi-target BR estimation; (c), (d) accuracy on multi-target HR estimation; (e), (f) errors for multi-target BR estimation; (g), (h) errors for multi-target HR estimation. X-axis: subject-to-radar distance. The angle separation between subjects is  $60^{\circ}$ .

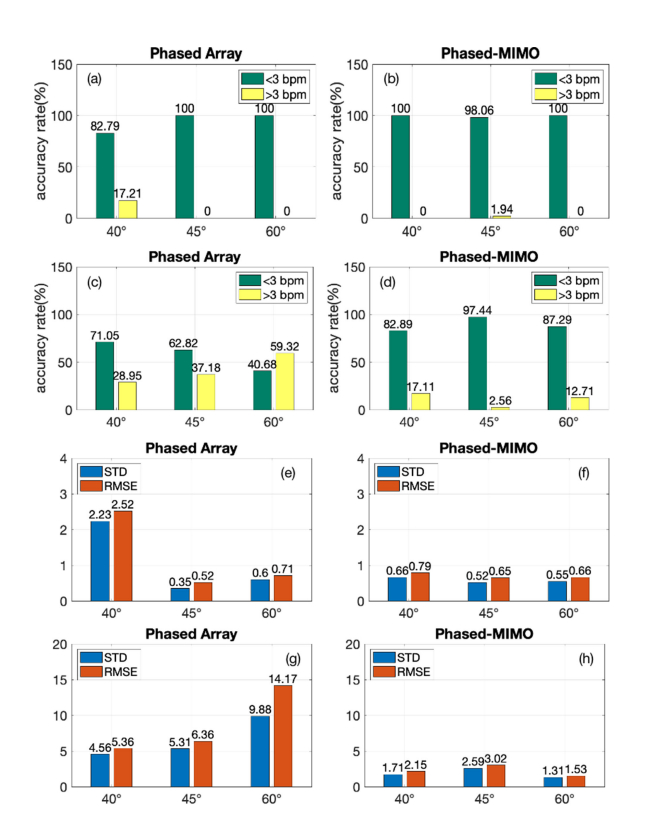


Fig. 11. (a), (b) Accuracy on multi-target BR estimation; (c), (d) accuracy on multi-target HR estimation; (e), (f) errors for multi-target BR estimation; (g), (h) errors for multi-target HR estimation. X-axis: angle between two targets. The radar-to-target distances are all  $1.6\ m$ .

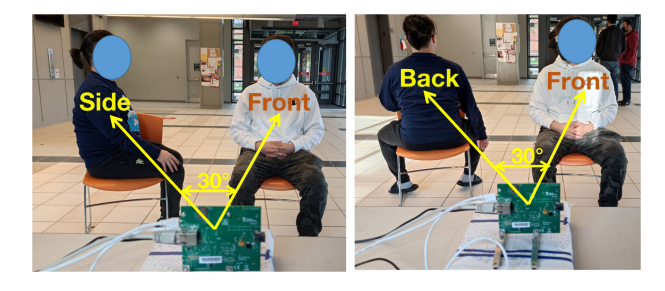


Fig. 12. Experiment setup for different targets' orientations.

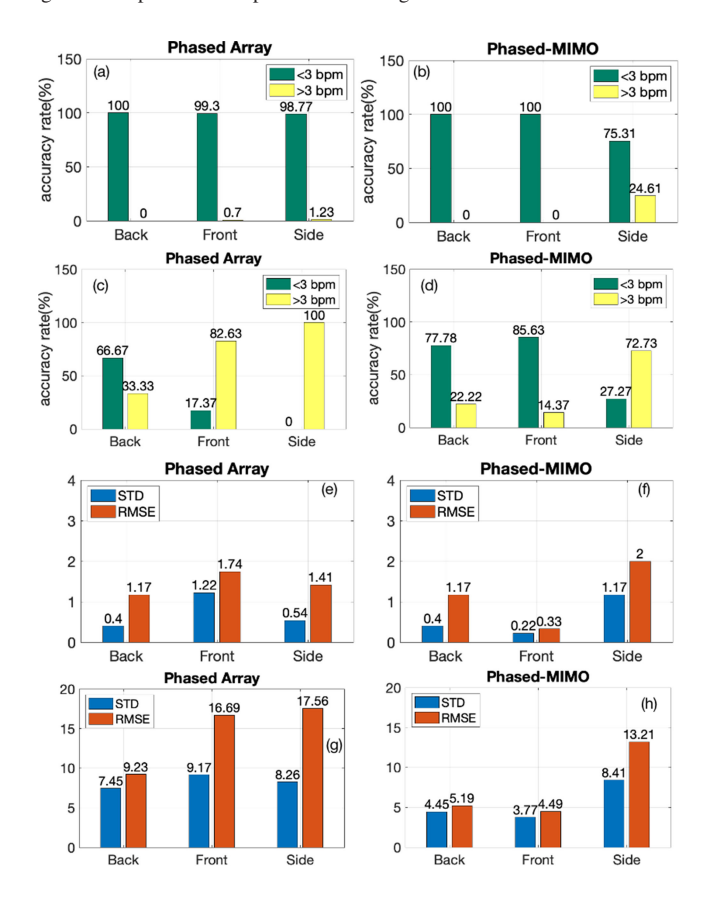


Fig. 13. (a), (b) Accuracy on multi-target BR estimation; (c), (d) accuracy on multi-target HR estimation; (e), (f) errors for multi-target BR estimation; (g), (h) errors for multi-target HR estimation. X-axis: target orientations. The radar-to-target distances are all  $1.6\ m$  and inter-target angle is  $30^{\circ}$ .

phased array is larger than 82.79% while the accuracy rate of the phased-MIMO is larger than 98.06% when the angle separation is changed from 40° to 60°. For HR measurement shown in Figs. 11(c) and (d), the accuracy rate for the phased array is larger than 62.82% while the accuracy rate for the phased-MIMO is larger than 82.89% when the angle separation is changed from 40° to 60°. Furthermore, Figs. 11(e) and (f) show that the STD and RMSE results for phased-MIMO are smaller than those for phased array. Similar results can be seen in Figs. 11(g) and (h). For HR estimation, the accuracy rates for the phased-MIMO are larger than those for the phased array under different angle separations.

Further experiments were conducted with targets not facing the radar; the setup is shown in Fig. 12. Figs. 13(a) and (b) show the performance of BR estimation based on the phased array and the phased-MIMO, while Figs. 13(c) and (d) illustrate the HR

estimation performance. Figs. 13(e), (f), (g) and (h) show STD and RMSE results for the phased array and the phased-MIMO in this case, respectively. As can be seen in Fig. 13, when the radar sensor is used to detect vital sign signals on the front and back chest of target, the accuracy rates for either the phased array or the phased-MIMO are higher than those when the radar sensor is located on the right side of target. This is mainly because, in this case, the chest displacement is not obvious on the arm. Furthermore, the reflection area becomes much smaller in that orientation, thus the breathing and heartbeat are much more difficult to detect when the radar sensor is located on the right side of target.

It needs to be mentioned that, an experiment where two targets are at same radial distance of 1.6 m and angle separation of  $20^\circ$  was also conducted. In this case, the proposed phased-MIMO can resolve and accurately estimate the different breathing rates of the two targets while the heart rates can not be resolved. In our future work, more advanced radar techniques, e.g., CB at transmitter side, would be applied to improve the performance of the propose system on more challenging scenarios, e.g., larger subject-to-radar distance and smaller subject-to-subject distance.

#### V. CONCLUSION

We have designed a TDM phased-MIMO radar to realize high-precision multi-people vital sign monitoring. The designed radar can successively steer the mmWave beam towards different directions, which enables the separation of vital signals of multiple subjects at the same range bin and integrates the MIMO technique into our design to boost the SNR. The received echoes are processed with Capon's beamformer to further enhance the directivity which allows us to localize multiple target subjects and extract echoed mmWave signals of each individual subject. As compared to the phased array, our TDM-phased MIMO with receive beamforming can more accurately estimate the BR and the HR of multiple subjects. Furthermore, compared to the state-of-the-art MIMO-based approach [12], which relies on a large antenna array (i.e., with 192 TX-RX antenna pairs), our solution achieves similar performance with the approach to BR detection (0.1 RMSE vs 0.2 RMSE) and HR estimation (0.6 RMSE vs 0.53 RMSE) in single target scenario while using a smaller array of only 8 TX-RX pairs. We believe that by implementing our method on the large antenna array used in [12], the performance of vital signal monitoring could be further improved. In [27], due to high attenuation of mmWave signal, the detection is within 2m. Here in our work, with analog beamforming at transmitter side, the vital signal can be detected at a longer distance of 4m. We believe that performance can also be improved by combining the phased-MIMO radar with sophisticated signal processing techniques.

### REFERENCES

- F.-K. Wang et al., "Review of self-injection-locked radar systems for noncontact detection of vital signs," *IEEE J. Electromagn.*, RF, Microw. Med. Biol., vol. 4, no. 4, pp. 294–307, Dec. 2020.
- [2] Y. Yuan, A. Y.-K. Chen, and C.-T. M. Wu, "A high-sensitivity low-power vital sign radar sensor based on super-regenerative oscillator architecture," in *Proc. IEEE/MTT-S Int. Microw. Symp.*, 2020, pp. 651–654.
- [3] A. Rahman, E. Yavari, X. Gao, V. Lubecke, and O. Boric-Lubecke, "Signal processing techniques for vital sign monitoring using mobile short range doppler radar," in *Proc. IEEE Topical Conf. Biomed. Wireless Technol.*, *Netw., Sens. Syst.*, 2015, pp. 1–3.

- [4] C. Gu, G. Wang, Y. Li, T. Inoue, and C. Li, "A hybrid radar-camera sensing system with phase compensation for random body movement cancellation in doppler vital sign detection," *IEEE Trans. Microw. Theory Techn.*, vol. 61, no. 12, pp. 4678–4688, Dec. 2013.
- [5] F. Adib, H. Mao, Z. Kabelac, D. Katabi, and R. C. Miller, "Smart homes that monitor breathing and heart rate," in *Proc. Annu. ACM Conf. Hum. Factors Comput. Syst.*, 2015, pp. 837–846.
- [6] J. Liu, Y. Wang, Y. Chen, J. Yang, X. Chen, and J. Cheng, "Tracking vital signs during sleep leveraging off-the-shelf WiFi," in *Proc. ACM Int. Symp. Mobile Ad Hoc Netw. Comput.*, 2015, pp. 267–276.
- [7] M. Mercuri, Y.-H. Liu, I. Lorato, T. Torfs, A. Bourdoux, and C. V. Hoof, "Frequency-tracking CW doppler radar solving small-angle approximation and null point issues in non-contact vital signs monitoring," *IEEE Trans. Biomed. Circuits Syst.*, vol. 11, no. 3, pp. 671–680, Jun. 2017.
- [8] A. Ahmad, J. C. Roh, D. Wang, and A. Dubey, "Vital signs monitoring of multiple people using a FMCW millimeter-wave sensor," in *Proc. IEEE Radar Conf.*, 2018, pp. 1450–1455.
- [9] M. Alizadeh, G. Shaker, J. C. M. D. Almeida, P. P. Morita, and S. Safavi-Naeini, "Remote monitoring of human vital signs using mm-wave FMCW radar," *IEEE Access*, vol. 7, pp. 54958–54968, 2019.
- [10] T. Sakamoto and K. Yamashita, "Noncontact measurement of autonomic nervous system activities based on heart rate variability using ultrawideband array radar," *IEEE J. Electromagn., RF, Microw. Med. Biol.*, vol. 4, no. 3, pp. 208–215, Sep. 2020.
- [11] S. M. Islam, N. Motoyama, S. Pacheco, and V. M. Lubecke, "Non-contact vital signs monitoring for multiple subjects using a millimeter wave FMCW automotive radar," in *Proc. IEEE/MTT-S Int. Microw. Symp.*, 2020, pp. 783–786.
- [12] T. K. Vodai et al., "Enhancement of remote vital sign monitoring detection accuracy using multiple-input multiple-output 77 GHz FMCW radar," IEEE J. Electromagn., RF, Microw. Med. Biol., to be published, doi: 10.1109/JERM.2021.3082807.
- [13] W.W. Lv, X. H.Lin, and J. Miao, "Non-contact monitoring of human vital signs using FMCW millimeter wave radar in the 120 GHz band," *Sensors*, vol. 21, no. 8, 2021, Art. no. 2732. [Online]. Available: https://www.mdpi. com/1424-8220/21/8/2732
- [14] J.-M. Muñoz-Ferreras, J. Wang, Z. Peng, C. Li, and R. Gómez-García, "FMCW-radar-based vital-sign monitoring of multiple patients," in *Proc. IEEE MTT-S Int. Microw. Biomed. Conf.*, 2019, vol. 1, pp. 1–3.
- [15] E.J. M. Turppa, O. K.Antropov, and T. Kiuru, "Vital sign monitoring using FMCW radar in various sleeping scenarios," Sensors, vol. 20, no. 22, 2020, Art. no. 6505. [Online]. Available: https://www.mdpi.com/1424-8220/20/ 22/6505
- [16] Y. Xiong, S. Li, C. Gu, G. Meng, and Z. Peng, "Millimeter-wave bat for mapping and quantifying micromotions in full field of view," *Research*, vol. 2021, 2021, Art. no. 9787484.
- [17] M. Mercuri, I. R. Lorato, Y.-H. Liu, F. Wieringa, C. V. Hoof, and T. Torfs, "Vital-sign monitoring and spatial tracking of multiple people using a contactless radar-based sensor," *Nature Electron.*, vol. 2, no. 6, pp. 252–262, 2019.
- [18] J. Li and P. Stoica, MIMO Radar Signal Processing. Hoboken, NJ, USA: Wiley, 2008.
- [19] S. M. Patole, M. Torlak, D. Wang, and M. Ali, "Automotive radars: A review of signal processing techniques," *IEEE Signal Process. Mag.*, vol. 34, no. 2, pp. 22–35, Mar. 2017.
- [20] A. De Groote, M. Wantier, G. Cheron, M. Estenne, and M. Paiva, "Chest wall motion during tidal breathing," J. Appl. Physiol., vol. 83, no. 5, pp. 1531–1537, 1997. [Online]. Available: https://doi.org/10.1152/jappl. 1997.83.5.1531
- [21] M. Mabrouk, S. Rajan, M. Bolic, M. Forouzanfar, H. R. Dajani, and I. Batkin, "Human breathing rate estimation from radar returns using harmonically related filters," *J. Sensors*, vol. 2016, pp. 1252–1258, 2016.
- [22] Y. Wang, W. Wang, M. Zhou, A. Ren, and Z. Tian, "Remote monitoring of human vital signs based on 77-GHz mm-wave FMCW radar," *Sensors*, vol. 20, 2020, Art. no. 2999.
- [23] Texas Instrument, "AWR2243 Evaluation module (AWR2243BOOST) mmWave sensing solution," 2020.
- [24] Texas Instrument, "MIMO radar," TI Appl. Rep. SWRA554 A, 2018.
- [25] Texas Instrument, "DCA1000EVM real-time data-capture adapter for radar sensing evaluation module," Rep. SPRUIJ4A, 2019.
- [26] Texas Instrument, "Programming chirp parameters in ti radar devices," Appl. Rep. SWRA553 A, 2020.
- [27] F. Wang, F. Zhang, C. Wu, B. Wang, and K. J. R. Liu, "ViMo: Multiperson vital sign monitoring using commodity millimeter-wave radiotexas instrument," *IEEE Internet Things J.*, vol. 8, no. 3, pp. 1294–1307, 2021.

- [28] S. Sun, A. P. Petropulu, and H. V. Poor, "MIMO radar for advanced driver-assistance systems and autonomous driving: Advantages and challenges," *IEEE Signal Process. Mag.*, vol. 37, no. 4, pp. 98–117, 2020, doi: 10.1109/MSP.2020.2978507.
- [29] J. Wang, X. Wang, L. Chen, J. Huangfu, C. Li, and L. Ran, "Noncontact distance and amplitude-independent vibration measurement based on an extended DACM algorithm," *IEEE Trans. Instrument. Measur.*, vol. 63, no. 1, pp. 145–153, Jan. 2014, doi: 10.1109/TIM.2013.2277530..



Zhaoyi Xu (Graduate Student Member, IEEE) received the B.E degree in electrical engineering from the University of Electronic Science and Technology of China, Chengdu, China, in 2018. He is currently working toward the Ph.D. degree with the Department of Electronics and Communication Engineering, Rutgers University, New Brunswick, NJ, USA, with Prof. Athina Petropulu. His research interests include radar signal processing, sparse array design, dual function radar communication system design, and remote vital signal monitoring.



**Cong Shi** is currently working toward the Ph.D. degree with Wireless Information Network Lab, Rutgers University, New Brunswick, NJ, USA.

He was the recipient of the two industry-sponsored fellowships by Cisco System and Siemens Corporate Research. He is with Data Analysis and Information Security Lab, led by Prof. Yingying (Jennifer) Chen. His research interests include cyber security and privacy, mobile sensing, smart healthcare, Internet of Things, security in machine learning, and artificial intelligence.



**Tianfang Zhang** was born in Weifang, China, on September 28, 1996. He received the B.E degree in information security from the Huazhong University of Science and Technology, Wuhan, China, in 2019, and the M.S. degree in computer science in 2021 from Rutgers University, New Brunswick, NJ, USA, where he is currently working toward the Ph.D. degree. His research interests include machine learning, mobile system, wireless sensing, and cyber security.



Shuping Li (Graduate Student Member, IEEE) was born in Liaoning Province, China, on November 20, 1997. He received the B.Sc. degree in electrical engineering from the University of Electronic Science and Technology of China, Chengdu, China, in 2019, and the M.Sc. degree in electrical engineering in 2020 from Rutgers University, New Brunswick, NJ, USA, where he is currently working toward the Ph.D. degree. His research focuses on electromagnetic metamaterial antenna based radar sensor designs.



Yichao Yuan (Student Member, IEEE) was born in Lanzhou, China, in June 1992. He received the B.Sc. and M.Sc. degrees in electrical engineering from Tongji University, Shanghai, China, in 2014 and 2017, respectively. He is currently working toward the Ph.D. degree with Rutgers University, New Brunswick, NJ, USA. From June 2021 to August 2021, he was an Antenna Engineering Intern with Tesla, Inc., Palo Alto, CA, USA. His research focuses on electromagnetic metamaterial antenna-based radar sensor designs.



Chung-Tse Michael Wu (Senior Member, IEEE) received the B.S. degree in electrical engineering from National Taiwan University, Taipei, Taiwan, in 2006, and the M.S. and Ph.D. degrees in electrical engineering from the University of California at Los Angeles, Los Angeles, CA, USA, in 2009 and 2014, respectively.

From September 2008 to June 2014, he was a Graduate Student Researcher with the Microwave Electronics Laboratory, UCLA. In 2009, he was a

Summer Intern with Bell Labs, Murray Hills, NJ, USA. In 2012, he was a Special-Joint Researcher with the Japan Aerospace Exploration Agency, Sagamihara, Japan. From 2014 to 2017, he was an Assistant Professor with the Department of Electrical and Computer Engineering, Wayne State University, Detroit, MI, USA. He is currently an Assistant Professor with Rutgers University, New Brunswick, NJ, USA. His research interests include applied electromagnetics, antennas, passive/active microwave and millimeterwave components, RF systems, and metamaterials.

Dr. Wu is currently the Vice Chair of the IEEE Princeton Central Jersey Section, and the Vice Chair of the IEEE PCJS joint AP/ED/MTT chapter. He is also the Chair and a Technical Program Committee Member of the IEEE MTT-28: Biological Effects and Medical Applications of RF and Microwaves. He was the recipient of the National Science Foundation (NSF) Faculty Early Career Development (CAREER) Award, WSU College of Engineering Faculty Research Excellence Award in 2016, Defense Advanced Research Projects Agency (DARPA) Young Faculty Award (YFA) in 2019, and DARPA Director's Fellowship Award in 2021.



Yingying Chen (Fellow IEEE) is currently a Professor of electrical and computer engineering and Peter Cherasia Endowed Faculty Scholar with Rutgers University, New Brunswick, NJ, USA. She is the Associate Director of the Wireless Information Network Laboratory. She also leads the Data Analysis and Information Security Lab. She has authored or coauthored more than three books, four book chapters and more than 200 journal articles and refereed conference papers. Her research interests include mobile sensing and computing, cyber security and privacy,

Internet of Things, and smart healthcare. Previously, she had extensive industry experiences with Nokia. Her research has been reported by numerous media outlets.

She is the NAI Fellow. She is serving/served on the editorial boards of the IEEE/ACM TRANSACTIONS ON NETWORKING, IEEE TRANSACTIONS ON MOBILE COMPUTING, IEEE TRANSACTIONS ON WIRELESS COMMUNICATIONS, and ACM Transactions on Privacy and Security. She was the recipient of seven best paper awards in top ACM and IEEE conferences.



Athina Petropulu (Fellow IEEE) is currently a Distinguished Professor with the Department of Electrical and Computer Engineering, Rutgers University, New Brunswick, NJ, USA, and was the Chair of the Department during 2010–2016. Prior to joining Rutgers University, she was a Professor of electronics and communication engineering with Drexel University, Philadelphia, PA, USA, during 1992–2010. She held Visiting Scholar appointments with SUPELEC, Universite' Paris Sud, Orsay, France, Princeton University, Princeton, NJ, USA, and University of South-

ern California, Los Angeles, CA, USA. Her research interests include statistical signal processing, wireless communications, signal processing in networking, physical layer security, and radar signal processing. Her research has been funded by various government industry sponsors, including the National Science Foundation, Office of Naval research, U.S. Army, National Institute of Health, Whitaker Foundation, Lockheed Martin and Raytheon. Dr. Petropulu is Fellow of the American Association for the Advancement of Science. She is 2022-2023 President of the IEEE Signal Processing Society and 2020-2021 President-Elect of IEEE SPS. She has was the Editor-in-Chief of the IEEE TRANSACTIONS ON SIGNAL PROCESSING during 2009-2011 and IEEE Signal Processing Society Vice President-Conferences during 2006-2008. She was the General Chair of the 2020 and 2021 IEEE SPS PROGRESS Workshops, the General Co-Chair of the 2018 IEEE International Workshop on Signal Processing Advances in Wireless Communications, Kalamata Greece, and the Genera Chair of the 2005 International Conference on Acoustics Speech and Signal Processing, Philadelphia, PA, USA. She was a Distinguished Lecturer of the Signal Processing Society from 2017 to 2018, and is currently a Distinguished Lecturer of the IEEE Aerospace and Electronics Systems Society. She was the recipient of the 1995 Presidential Faculty Fellow Award given by NSF and the White House, 2012 IEEE Signal Processing Society Meritorious Service Award, and co-recipient of the 2005 IEEE Signal Processing Magazine Best Paper Award, 2020 IEEE Signal Processing Society Young Author Best Paper Award (B. Li), 2021 IEEE Signal Processing Society Young Author Best Paper Award (F. Liu), and 2021 Barry Carlton Best Paper Award by IEEE Aerospace and Electronic Systems